1

Transformation of polyvinyl chloride (PVC) into a versatile and efficient adsorbent of Cu(II) cations and Cr(VI) anions through hydrothermal treatment and sulfonation

3 Xianbao Xu[a], Daan Zhu[a], Xiaonuan Wang[a], Liling Deng[a], Xinyun Fan[d], Zizhen Ding[a], Ai

4 Zhang[a], Gang Xue[a], Yanbiao Liu[a], Weimin Xuan[c], Xiang Li[a, *], Jacek Makinia[b]

5 *a College of Environmental Science and Engineering, State Environmental Protection*

6 *Engineering Centre for Pollution Treatment and Control in Textile Industry, Donghua*

7 *University, 2999 North Renmin Road, Shanghai 201620, China*

8 *b Faculty of Civil and Environmental Engineering, Gdansk University of Technology, ul.*

9 *Narutowicza 11/12, 80-233 Gdansk, Poland*

10 *c College of Chemistry, Chemical Engineering and Biotechnology, Donghua University, 2999*

11 *North Renmin Road, Shanghai 201620, China*

12 *d State Key Laboratory of Pollution Control and Resources Reuse, School of Environmental*

13 *Science and Engineering, Tongji University, 1239 Siping Road, Shanghai 200092, China*

14

15

16 *Corresponding author

17 E-mail: lix@dhu.edu.cn

18 Tel: 86-21-67792538

19 Fax: 86-21-67792159

20

Abstract

The reuse of waste polyvinyl chloride (PVC) has drawn much attention as it can reduce plastic waste and associated pollution, and provide valuable raw materials and products. In this study, sulfonated PVC-derived hydrochar (HS-PVC) was synthesized by two-stage hydrothermal treatment (HT) and sulfonation, and shown to be a versatile adsorbent. The reoval of Cu(II) cations and Cr(VI) anions using HS-PVC reached $81.2 \pm 1.6\%$ and $60.3 \pm 3.8\%$, respectively. The first stage of HT was crucial for the dichlorination of PVC and the formation of an aromatic structure. This stage guaranteed the introduction of $-SO_3H$ onto PVC-derived hydrochar through subsequent sulfonation. HT intensities (i.e., temperature and time) and sulfonation intensity strongly determined the adsorption capacity of HS-PVC. Competitive adsorption between Cu(II) and Cr(VI) onto HS-PVC was demonstrated by binary and preloading adsorption. The proposed Cu(II) cations adsorption mechanism was electrostatic adsorption, while Cr(VI) were possibly complexed by the phenolic -OH and reduced to Cr(III) cations by C=C groups in HS-PVC. In addition, HS-PVC derived from PVC waste pipes performed better than PVC powder for Cu(II) and Cr(VI) removal (> 90%). This study provides an efficient method for recycling waste PVC and production of efficient adsorbents.

Keywords: Polyvinyl chloride; Hydrothermal treatment; Sulfonation; Adsorption; Cu(II) cations and Cr(VI) anions

1. Introduction

Polyvinyl chloride (PVC) is irreplaceable in the infrastructure of modern society (Cui et al., 2021). However, large quantities of plastic waste continuously enter aquatic and terrestrial ecosystems, leading to ubiquitous pollution worldwide (Kawecki and Nowack 2019, Miao et al., 2020). For example, the accumulated PVC waste in China will exceed 500 million tons by the end of 2050, posing a daunting challenge for the safe and effective disposal of this halogenated waste (Liu et al., 2020).

Mechanical recycling (25.5%), incineration (9.3%), and landfill disposal (36.0%) are currently the main solutions for solving the problem of PVC waste (Yu et al., 2016, Ye et al., 2017, Liu et al., 2020). However, mechanical recycling is still rudimentary and only suitable for source-separated PVC waste. Incineration and landfill disposal of PVC waste normally release hazardous compounds, such as polychlorinated dibenzo-p-dioxins and polychlorinated dibenzofurans. Furthermore, the land requirements of landfills must be considered (Wiedinmyer et al., 2014). Thus, reliable alternative methods to treat PVC waste safely and efficiently in an environmentally sound and high value-added way are worth pursuing (Lau et al., 2020). Such an approach is in line with the European Union's strategy for plastics in a circular economy (Matthews et al., 2021).

Hydrothermal treatment (HT), conducted at relatively low temperatures of 160 to 300°C, can pretreat PVC waste for dehydrochlorination (Ma et al., 2019, Ning et al., 2020), permitting subsequent pyrolysis to produce chars and liquid hydrocarbons with a low Cl content, such as alkene and polyene (Poerschmann et al., 2015, Jiang et al., 2021). However,

63   cost- and energy-intensive conditions, such as noble metal catalysts and high temperature

64   (500℃), are typically adopted for lighter oil production by catalytic pyrolysis of plastic

65   (Kunwar et al., 2016, Maity et al., 2020). On the other hand, PVC waste can be converted

66   into coal-alternative fuels by HT processes amended with cellulose (Shen et al., 2017),

67   pinewood sawdust (Huang et al., 2019), and corncob (Lu et al., 2020). Yet, another important

68   recycling method has been undervalued and ignored, i.e., the potential transformation of

69   PVC-derived hydrochar (H-PVC) into an effective adsorbent for the removal of contaminants,

70   such as heavy metals.

71   Unfortunately, the adsorption capacity of organic compounds by H-PVC is very low,

72   primarily because surface-related adsorption prevails over hydrophobic partitioning

73   (Poerschmann et al., 2015). Several studies showed that the adsorption of hydrochar derived

74   from natural biomass sources was enhanced by introducing functional groups, such as $-OH$,

75    $-COOH$, and $-NH_2$, which could trap heavy metal ions from aqueous solutions (Azzaz et al.,

76   2020, Yang et al., 2021). Sulfonation is an attractive modifications method for various carbon

77   materials due to the unique surface chemistry and low production costs. Large amounts of

78   oxygen functionalities, such as $-OH$, $-COOH$, and lactones, along with $-SO_3H$ groups, are

79   introduced into the surface of the carbon materials, improving their hydrophilic/oxyphilic

80   properties after sulfonation. Sulfonated carbon materials have been widely applied in the

81   catalysis of esterifications, acetalization, etherifications, and transesterifications (Konwar et

82   al., 2019). However, sulfonated PVC-derived hydrochar (HS-PVC) has rarely been reported,

83   albeit potentially being a cost-effective adsorbent for heavy metals.

84   The novelty of the present work is the development of two-stage HT and sulfonation to

85   synthesize PVC-derived adsorbents for the removal of both Cu(II) cations and Cr(VI) anions.

86   A systematic investigation was conducted to discern the mechanisms underlying functional

87   group modifications of PVC through different strategies and treatment intensities. The

88   adsorption mechanisms of Cu(II) and Cr(VI) were clarified to understand the adsorption

89   behavior onto HS-PVC. The performance of HS-PVC to adsorb Cu(II) and Cr(VI) from

90   natural water was evaluated. PVC waste pipes were used to synthesize HS-PVC and test its

91   applications. Furthermore, the versatility of HS-PVC for the adsorption of low concentrations

92   of Cu(II) and Cr(VI) (20 mg/L) and other metals, i.e., Mn(II), Cd(II), Ni(II), and Co(II) was

93   investigated. This study provides a practical approach for the sustainable reuse of waste PVC

94   as an efficient adsorbent to remove heavy metal cations and anions.

95

96   **2. Materials and methods**

97   **2.1. Preparation of PVC-derived adsorbents**

98   Raw PVC powder (sieved through a 100 mesh) was purchased from a plastic chemical

99   company (Guangdong, China). Hydrothermal batch reactions were conducted by loading 10 g

100   of Raw PVC with 40 mL distilled water in 100-mL airtight stainless-steel tubular reactors

101   with internal polyphenylene containers. The reactors were heated to 250 °C for 6 h in a

102   homothermic oven (DHG-9013A, China). The reactors were then cooled to room temperature

103   in a water bath to prepare the H-PVC. Ten grams of Raw PVC was sulfonated in flasks (250

104   ml) with concentrated sulfuric acid (98%) at a sulfonation intensity of 1:10 (g/mL) in a shaking

105   bath (70 °C and 110 rpm for 12 h) to produce the sulfonated PVC (S-PVC). Unless otherwise

106   specified, sulfonation intensity refers to the ratio of adsorbent mass to the volume of sulfuric

107   acid in this paper. Specifically, a relatively low temperature of sulfonation (70 °C) was chosen

108   according to the literature (Xiao and Hill 2020). The HS-PVC was synthesized by sulfonation

109   of H-PVC with the same process as described for S-PVC. The S-PVC and HS-PVC were

110   washed three times with distilled water to eliminate the unreacted sulfuric acid. The Raw PVC,

111   H-PVC, S-PVC, and HS-PVC were dried in a homothermic oven at 105 °C for 24 h. The dried

112   PVC-derived adsorbents were then ground and sieved through a 100 mesh (147 um) before

113   adsorption of Cu(II) and Cr(VI).

2.2. PVC-derived adsorbents for highly efficient removal of Cu(II) and Cr(VI)

2.2.1. Cu(II) and Cr(VI) removal using Raw PVC, H-PVC, S-PVC, and HS-PVC

116   A stock solution of 500 mg Cu(II)/L (7.87 mM) was prepared by dissolving 1965 mg of

117   copper sulfate pentahydrate (CuSO$_4$·5H$_2$O) in 1 L of ultrapure water. A stock solution of 250

118   mg Cr(VI)/L (4.81 mM) was prepared by dissolving 770 mg of potassium dichromate

119   (K$_2$Cr$_2$O$_7$) in 1 L of ultrapure water. Batch experiments of Cu(II) and Cr(VI) removal were

120   performed by adding 10 g/L of Raw PVC, H-PVC, S-PVC, and HS-PVC to flasks (250 mL)

121   in a water bath shaker (25 °C and 100 rpm) for 12 h. All samples were withdrawn from the

122   flasks and filtered through membrane filters with a pore size of 0.22 μm for subsequent Cu(II)

123   and Cr(VI) determination.

124   The removal efficiencies of Cu(II) and Cr(VI) were calculated as:

125   Removal efficiency $= \frac{c_0 - c_t}{c_0} \times 100\%$ $\quad\quad\quad\quad\quad\quad\quad\quad\quad$ (1)

126   where C_0 (mg/L) and C_t (mg/L) were the concentrations of Cu(II) and Cr(VI) at the start

127   of the experiment and time t (h). Unless otherwise specified, all calculations of Cu(II) and

128   Cr(VI) removal efficiencies by PVC-derived adsorbents followed this equation. The

129   concentrations of Cu(II) and Cr(VI) were determined by inductively coupled plasma mass

130   spectrometry (ICP-MS) (Thermo Scientific iCAP Q, USA).

131   **2.2.2. Cu(II) and Cr(VI) removal using HS-PVC under different intensities of HT**

132   **temperature, HT time, and sulfonation and correlation analyses**

133   HS-PVC was synthesized under different intensities of HT (temperature and time) and

134   sulfonation as follows: HT temperatures from 220 °C to 260 °C (in 10 °C intervals, HT time

135   of 6 h and sulfonation intensity of 1:10), HTC times from 2 h to 6 h (in 1 h intervals, HT

136   temperature of 250 ℃, and sulfonation intensity of 1:10), and sulfonation intensities from 1:1

137   to 1:10 (in 1:10 intervals, HT temperature of 250 ℃, and HT time of 6 h). 10 g/L HS-PVC

138   fabricated with different HT intensities and sulfonation were used for Cu(II) and Cr(VI)

139   removal at 25 °C and 100 rpm. To investigate the individual effects of the intensities of HT

140   temperature, HT time, and sulfonation on Cu(II) and Cr(VI) removal, enhancements of Cu(II)

141   and Cr(VI) removal were calculated by comparing the lowest value with the highest one (250 °C

142   vs. 220°C, 6 h vs. 2 h, and 1:10 vs. 1:1, respectively).

143   **2.2.3. Adsorption kinetics and isotherms of Cu(II) and Cr(VI) removal using HS-PVC**

144   The adsorption kinetics of Cu(II) and Cr(VI) removal were studied based on the removal

145   efficiencies of HS-PVC as described in Section 2.2.1. Adsorption isotherm experiments were

146   carried out with different initial concentrations of Cu(II) (i.e., 100, 200, 300, 400, 500, 600,

147 and 800 mg/L) and Cr(VI) (50, 100, 150, 200, 250, and 300 mg/L) at three different

148 temperatures (25, 35, and 45 °C) using 10 g/L HS-PVC under optimum operational

149 conditions (250°C, 6 h, and a sulfonation intensity of 1:10).

150 Pseudo-first-order (PFO) and pseudo-second-order (PSO) models were used to evaluate

151 Cu(II) and Cr(VI) removal kinetics of HS-PVC, and their linearized equations are given in

152 *Eqs.* (2) and (3), respectively.

153 $\ln(q_e - q_t) = \ln q_e - k_1 t$ (2)

154 $\frac{t}{q_t} = \frac{1}{k_2 q_e^2} + \frac{t}{q_e}$ (3)

155 where k_1 and k_2 are the rate constants of PFO and PSO, respectively, and q_e and q_t (mg/g)

156 are the amounts of adsorbed Cu(II) and Cr(VI) (mg/g) at equilibrium and at time t,

157 respectively. Values of k_1, k_2, and q_e were calculated based on the Levenberg-Marquardt

158 method at the 95% confidence level.

159 To predict the adsorption capacity of the adsorbents, two widely used isotherms (i.e.,

160 Langmuir and Freundlich) were selected among several models. *Eqs*. (4) and (5) express the

161 Langmuir isotherm and the Freundlich isotherm, respectively.

162 $q_e = \frac{b q_m C_e}{1 + b C_e}$ (4)

163 $q_e = K_F C_e^{1/n}$ (5)

164 where q_m (mg/g) is the maximum adsorption capacity of the adsorbent and b (L/mg) is

165 the Langmuir constant related to the adsorption energy. K_F (mg/g) is the Freundlich

166 adsorption isotherm constant related to the extent of adsorption and n is the heterogeneity

167 factor of the Freundlich model. Values of b, q_m, K_F, and n were also calculated based on the

168   Levenberg-Marquardt method at the 95% confidence level.

169   **2.2.4. Competitive adsorption of Cu(II) and Cr(VI) onto HS-PVC in binary solution and**

170   **preloading adsorption**

171   Binary adsorption of Cu(II) and Cr(VI) was carried out by adding 10 g/L of HS-PVC to

172   a binary solution with 500 mg Cu(II)/L and 250 mg Cr(VI)/L in the same solution to

173   investigate the competitive adsorption between Cu(II) and Cr(VI). A separation factor was

174   utilized to investigate the adsorption selectivity in the binary solution, defined as:

175    $$\alpha_2^1 = \frac{q_{e1} \times C_{e2}}{C_{e1} \times q_{e2}} \qquad (6)$$

176   where q_{e1} (mmol/g) and C_{e1} (mmol/L) were the equilibrium adsorption capacity and

177   equilibrium concentration toward constituent 1, and q_{e2} (mmol/g) and C_{e2} (mmol/L) were the

178   equilibrium adsorption capacity and equilibrium concentration toward constituent 2,

179   respectively.

180   Preloading adsorption tests for Cr(VI) were performed by incubating 2.5 g HS-PVC in

181   250 mg/L Cr(VI) solution for 12 h. Then, the HS-PVC preloaded with Cr(VI) was used for

182   the adsorption of Cu(II) for 12 h, as described in Section 2.2.1. The preloading adsorption

183   tests for Cu(II) were performed under the same experimental conditions as those for Cr(VI).

184   The removal efficiencies of Cu(II) and Cr(VI) were calculated to evaluate the competitive

185   adsorption between Cu(II) and Cr(VI) onto the HS-PVC.

186   **2.2.5. Effect of K(I) on Cr(VI) removal**

187   The cations K(I) was present in the experimental Cr(VI) solutions prepared from

188    $K_2Cr_2O_7$. To assess the impact of K(I) on the adsorption of Cr(VI) by HS-PVC, $HClO_4$ (36.62

189 mL, calculated as described in Text S1) was added to precipitate K(I) (Ksp of KClO$_4$ 1.5×10^{-2})

190 in the Cr(VI) solution (total volume 100 mL). Then, HS-PVC (10 g/L) was added to the

191 treated Cr(VI) solution for adsorption for 12 h. Finally, the removal efficiency of Cr(VI) was

192 calculated to evaluate the impact of K(I) on the adsorption of Cr(VI) using HS-PVC.

2.2.6. Low concentration Cu(II) and Cr(VI) removal using HS-PVC

194 The concentrations of Cu(II) and Cr(VI) in industrial applications, such as electroplating,

195 leather tanning, and alloy manufacturing, range from 20 to 600 mg/L. Thus, 10 g/L of

196 HS-PVC was added to 20 mg/L Cu(II) and Cr(VI) solutions to evaluate its adsorption

197 performance for low concentrations of these heavy metals. The adsorption procedure was the

198 same as in Section 2.2.1.

2.2.7. Cu(II) and Cr(VI) removal in natural water

200 To test the potential interference of natural water regarding Cu(II) and Cr(VI) adsorption

201 on HS-PVC, natural water (untreated surface water) was sampled from the Jingyue Lake in

202 Donghua University, Shanghai, China. This water was used to prepare Cu(II) (500 mg/L) and

203 Cr(VI) (250 mg/L) solutions. 10 g/L of HS-PVC was added to these Cu(II) and Cr(VI)

204 solutions and incubated for 12 h at 25°C and 100 rpm.

2.2.8. Cu(II) and Cr(VI) removal using HS-PVC derived from PVC waste pipes

206 To test the applications of HS-PVC in Cu(II) and Cr(VI) removal, real PVC waste pipes

207 were used to prepare HS-PVC (real waste PVC). First, the PVC waste pipes were fragmented

208 with a crusher and then washed with tap water. Subsequently, 10 g/L of the pretreated

209 HS-PVC from pipes was added to Cu(II) (500 mg/L) and Cr(VI) (250 mg/L) solutions for 12

210　h adsorption (at 25°C and 100 rpm).

2.3. Characterizations of PVC-derived adsorbents

2.3.1. Characterizations of Raw PVC, H-PVC, S-PVC, and HS-PVC

213　　The surface properties of Raw PVC, H-PVC, S-PVC, and HS-PVC were characterized by

214　scanning electron microscopy (SEM) (HITACHI, S-4800, Japan) and contact angle

215　measurements (θ) (Kino, SL200KS, USA). The specific surface area and pore distribution of

216　Raw PVC, H-PVC, S-PVC, and HS-PVC were determined by the Brunauer−Emmett−Teller

217　(BET) (Quantachrome, Autosorb-iQ, USA) method and mercury intrusion porosimetry (MIP)

218　(Micromeritics, Auto pore lv, USA), respectively. Particle size distributions were calculated

219　based on the SEM images (Table S1). The elemental composition of Raw PVC, H-PVC,

220　S-PVC, and HS-PVC was analyzed by elemental analysis (Elementar, EL III, Germany) and

221　energy dispersive spectroscopic (EDS) (IE 300 X, England) element mapping. The variation

222　of functional groups of Raw PVC, H-PVC, S-PVC, and HS-PVC was characterized by Fourier

223　transform infrared (FTIR) spectroscopy (Thermo Fisher, NEX US-670, USA). The

224　thermostability of Raw PVC and HS-PVC was evaluated by thermogravimetric analysis (TGA,

225　TA, Netzsch, Germany).

2.3.2. Characterizations of HS-PVC before and after adsorption of Cu(II) and Cr(VI)

227　　The electric potentials of HS-PVC, HS-PVC after adsorption of Cu(II) (HS-PVC-Cu), and

228　HS-PVC after adsorption of Cr(VI) (HS-PVC-Cr) were determined by zeta potential

229　measurements (Brook Haven, 90 PALS, USA). In addition, the functional groups of HS-PVC

230　and HS-PVC-Cr were analyzed by X-ray photoelectron spectroscopy (XPS) (Thermo

231 Scientific, K-Alpha, USA), FTIR, solid-state ^{13}C nuclear magnetic resonance spectroscopy

232 (NMR) (Agilent, 600M, USA), and Raman spectroscopy (Thermo Fisher, DXR, USA). The

233 C1s XPS spectra were separated and characterized by C=C (284.8 eV), C-C (285.1 eV), C-O

234 (286.1 eV), and C=O groups (288.7 eV). The regions of functional groups derived from the

235 solid-state ^{13}C NMR spectra were divided into Carboxylic (220-161), Aromatic (161-113),

236 Anomeric (113-93), Carbohydrate (93-44), and Alkyl (44-0) (Wang et al., 2016, Li et al.,

237 2019).

238 **2.4. Statistical analysis**

239 All adsorption experiments were run in triplicate, and the results were expressed as

240 mean values ± standard deviation. The triplicate PVC-derived adsorbents were pooled to

241 minimize the potential variation before its characterizations (SEM, MIP, elemental analysis,

242 FTIR, TGA, XPS, solid-state ^{13}C NMR, and Raman spectroscopy). Analyses of variance

243 (ANOVA) were used to test for differences between treatments, and $p < 0.05$ was considered

244 statistically significant.

245

246 **3. Results and discussion**

247 **3.1. Highly efficient Cu(II) cations and Cr(VI) anions removal using HS-PVC**

248 Regarding Cu(II) removal, HS-PVC was significantly more efficient (81.2 ± 1.6%)

249 compared to Raw PVC (28.5 ± 1.7%) and PVC solely pretreated by either HT (14.5 ± 3.2%)

250 or sulfonation (20.6 ± 4.8%) within 12 h (Fig. 1A). In addition, HS-PVC was also highly

251 efficient in removing Cr(VI) (60.3 ± 3.8%) compared to Raw PVC (6.1 ± 1.3%) and PVC

252　solely pretreated by either HT (14.0 ± 4.6%) or sulfonation (7.0 ± 4.8%) within 12 h (Fig.

253　1B). The adsorption of Cu(II) reached equilibrium within 30 min while the adsorption

254　efficiency of Cr(VI) was only 49.3 ± 1.0% at 30 min and then slowly increased to equilibrium

255　within 3 h (Fig. S1). This suggested different adsorption mechanisms for Cu(II) and Cr(VI)

256　onto HS-PVC. Biomass-derived hydrochar was also widely employed in the adsorption of

257　metal cations, such as Cu(II), Zn(II), and Pb(II) (Deng et al., 2020, Kazak and Tor 2020, Song

258　et al., 2020) or metal anions, such as Cr(VI) ($Cr_2O_7^{2-}$) (Li et al., 2020). Cu(II) and Cr(VI)

259　could be simultaneously removed by hydrochar derived from chitosan with Fe_2O_3

260　modifications. However, the main adsorption mechanisms were chelation adsorption of Cu(II)

261　and electrostatic adsorption-coupled Cr(VI) reduction due to the specific dual-core Fe_2O_3@C

262　structure (Wang et al., 2017). The present study firstly provided a metal-free modification of

263　hydrochar derived from waste PVC for simultaneous Cu(II) cations and Cr(VI) anions

264　removal.

265　　　　The adsorption capacity of hydrochar was highly dependent on the functional groups

266　formed during HT (Tong et al., 2021). However, the structure and component of PVC

267　([-CH_2-CHCl-]n) were simpler compared to natural biomass, suggesting fewer functional

268　groups anchored in H-PVC than in natural biomass. This may explain why H-PVC is of little

269　significance for the adsorption of Cu(II) and Cr(VI) (Fig. 1), which was in line with poor

270　adsorption in wastewater remediation (Poerschmann et al., 2015). Sulfonation was also an

271　efficient modification of adsorbents derived from tea waste and cellulose for Cu(II) or Cr(VI)

272　removal (Dong et al., 2016, Ahsan et al., 2018). However, the adsorption of Cu(II) and Cr(VI)

273 using S-PVC was still low in this study. This paper showed a possible synergistic effect of

274 HT and sulfonation in the modifications of the methodology to produce a highly efficient

275 adsorbent.

3.2. Characterization during the fabrications of HS-PVC from Raw PVC in combination with HT and sulfonation

278 The microstructure of the PVC-derived adsorbents was characterized by SEM (Fig. 2A

279 to 2D). A rough surface and non-porous structures were observed in Raw PVC (Fig. 2A).

280 After HT treatment, the surface of H-PVC became smoother with an internal porous structure

281 (Fig. 2B) mainly due to dehydrochlorination, aromatization, and depolymerization reactions

282 during HT (Ning et al., 2020). There was no apparent difference between Raw PVC and

283 S-PVC in the SEM images (Fig. 2A and 2C), indicating that sulfonation possessed a marginal

284 impact on the surface structure. In contrast, the HS-PVC was fragmented with an internal

285 porous structure due to HT and sulfonation (Fig. 2D), which was consistent with a significant

286 decrease of particle size in HS-PVC compared to the Raw PVC (Fig. 3A and Table S2). In

287 addition, the hydrophobicity and hydrophilicity of adsorbents may influence the performance

288 of the adsorption process (Adam et al., 2020). The hydrophobicity of S-PVC was similar to

289 that of Raw PVC (Fig. 2E and 2G). However, the hydrophobicity was higher after HT (Fig.

290 2E and 2F), resulting in hydrophobic partitioning as described in the literature (Poerschmann

291 et al., 2015), which was consistent with the low adsorption efficiency of Cu(II) and Cr(VI) by

292 H-PVC (Fig. 1). Furthermore, the hydrophilicity of HS-PVC was significantly higher than

293 that of H-PVC (Fig. 2F and 2H), indicating that sulfonation improved the hydrophilicity of

HS-PVC, which is a prerequisite for the adsorption of Cu(II) and Cr(VI).

The BET surface areas of Raw PVC (2.59 m^2/g), H-PVC (4.95 m^2/g), S-PVC (2.01 m^2/g), and HS-PVC (0.59 m^2/g) (Table S3) were relatively low compared to those of biomass-derived hydrochar (118 m^2/g) in the literature (Sheng et al., 2019). According to the analysis of MIP (Fig. S2), the pore size in HS-PVC was mainly in the mesoporous (2-50 nm) and microporous (>50 nm) regions (Erdem et al., 2020, Rueda-Marquez et al., 2021). The results revealed that the Cu(II) and Cr(VI) adsorption mostly occurred in the mesoporous and microporous regions of the HS-PVC.

Elemental analysis (Fig. 3B) showed that the Cl/C molar ratio (0.5) of Raw PVC was similar to the stoichiometric value of ($[-CH_2-CHCl-]_n$). However, the molar ratio of Cl/C on the surface of Raw PVC (0.85 ± 0.37) was higher than 0.5 according to EDS element mapping (Fig. 3C), suggesting that most of the -Cl functional groups were on the surface of Raw PVC. The Cl/C ratio of H-PVC significantly decreased (Fig. 3B and 3C) compared to the Raw PVC after pretreatment by HT due to the dehydrochlorination (Poerschmann et al., 2015). The elemental composition of the entire Raw PVC and S-PVC was similar (Fig. 3B), but surface Cl was lower, and surface O slightly higher in S-PVC than in Raw PVC (Fig. 3C). This indicated that sole sulfonation only impacted the chemical composition on the surface of Raw PVC (Fig. 3C), causing no obvious chemical modifications to the entire Raw PVC (Fig. 3B). Additionally, the O/C and S/C ratios of HS-PVC increased, resulting in an O/S ratio of 3.04 (elemental analysis in Fig. 3B) or 3.16 (EDS element mapping in Fig. 3C). Thus, it could be hypothesized that the introduction of S-containing functional groups such as -SO_3H

315   (O/S=3) into HS-PVC occurred. The absorption peaks of HS-PVC from the FTIR at 1030

316   cm^{-1} (O=S=O) and 1169 cm^{-1} (-SO$_3$H) verified this assumption (Fig. 3D) (Chen et al., 2019).

317   The functional group -SO$_3$H was only detected in HS-PVC, indicating that the introduction of

318   -SO$_3$H onto HS-PVC was attributed to the synergy effect of HT and sulfonation. In addition,

319   the thermostability of HS-PVC was higher than that of Raw PVC according to the TGA

320   patterns (Fig. S3), which was mainly due to aromatization during HT (Park et al., 2016). It

321   has been reported that the presence of aromatic groups was essential for the sulfonation of

322   petroleum coke by concentrated H$_2$SO$_4$ (Xiao and Hill 2020). In this study, HT was crucial to

323   forming an aromatic structure (Fig. 3D) for the introduction of -SO$_3$H during sulfonation to

324   fabricate HS-PVC for highly efficient Cu(II) and Cr(VI) removal. Moreover, the functional

325   group C=C in HS-PVC (Fig. 3D) was crucial for removing Cr(VI), which was confirmed in

326   the following section.

327   **3.3. Correlations of Cu(II) and Cr(VI) removal with HT intensities and sulfonation**

328   The adsorption properties of HS-PVC were highly dependent on HT temperature and

329   time (see time curves in Fig. S4 and Fig. S5). The adsorption efficiencies of Cu(II) and Cr(VI)

330   increased from 36.9 ± 3.0% and 46.0 ± 3.8% at 220 °C to 81.1 ± 2.1% and 61.7 ± 2.7% at

331   250 °C, but declined to 63.7 ± 3.2% and 57.2 ± 1.3% at 260 °C, respectively (Fig. 4A). In

332   addition, the adsorption efficiencies of Cu(II) and Cr(VI) also increased from 56.5 ± 1.7%

333   and 9.2 ± 1.1% at 2 h to 80.0 ± 2.8% and 58.5 ± 1.1% at 6 h, followed by declines to 54.5 ±

334   2.0% and 2.2 ± 1.2% at 8 h, respectively (Fig. 4B). Higher HT intensities benefited PVC

335   dehydrochlorination (Zhang et al., 2020), providing more sites for subsequent SO$_3$H

336   introduction during sulfonation. It has been reported that proper HT intensities (HT

337   temperature = 250 °C and HT time = 6 h in this study) benefited the formation of the aromatic

338   structure (Ning et al., 2020). In contrast, higher HT intensities affected the stability of the

339   carbon structure (Ning et al., 2020), which explained the declines in the adsorptions of Cu(II)

340   and Cr(VI) onto HS-PVC at 260 °C (Fig. 4A) and 8 h (Fig. 4B).

341   The sulfonation intensity also affected the introduction of functional groups (Konwar et

342   al., 2019), thus affecting the adsorptive performance of HS-PVC. The adsorption time curves

343   of sulfonation intensity regarding Cu(II) and Cr(VI) removal by HS-PVC were shown in Fig.

344   S6. With the increasing sulfonation intensity, the adsorption efficiencies of Cu(II) and Cr(VI)

345   increased from $38.1 \pm 3.2\%$ and $28.4 \pm 3.5\%$ at the sulfonation intensity of 1:1 to $81.0 \pm 1.3\%$

346   and $59.6 \pm 2.4\%$ at the sulfonation intensity of 1:10 (Fig. 4C). The adsorption of Cu(II) and

347   Cr(VI) was positively correlated with the increase in sulfonation intensity from 1:1 to 1:10.

348   As summarized in Fig. 4D, the adsorption efficiency of Cu(II) increased by 117.4%

349   while that of Cr(VI) only by 34.1%, when increasing the temperature from 220 °C to 250 °C.

350   In contrast, the adsorption efficiency of Cu(II) improved only by 41.6%, while that of Cr(VI)

351   increased by 534%, with HT time increasing from 2 to 8 h. These results indicated that the

352   adsorption of Cu(II) was sensitive to HT temperature while the adsorption of Cr(VI) was

353   rather sensitive to HT time. However, the impact of sulfonation intensity on the adsorption of

354   Cu(II) (increasing 112.5% from 1:1 to 1:10) was similar to the adsorption of Cr(VI) (increasing

355   110.3% from 1:1 to 1:10).

3.4. Kinetics and isotherms of the adsorption of Cu(II) and Cr(VI) onto HS-PVC

356

357 Adsorption kinetics were essential to investigate the adsorption process (Song et al.,

358 2020, Wang and Guo 2020). The adsorption of Cu(II) and Cr(VI) onto the HS-PVC (Fig. 5A

359 and 5B) increased rapidly in the first 30 min and then decreased as the reaction approached

360 equilibrium due to the saturation of active adsorbent sites. The values of q_e and rate constants

361 (k_1 and k_2) obtained from the kinetic models (Fig. 5A and 5B) were shown in Table 1, along

362 with the correlation coefficients (R^2). The R^2 value of the PSO model was higher than that of

363 the PFO model for both Cu(II) and Cr(VI) adsorption. In addition, the q_e calculated by the

364 PSO model was more consistent with the experimental value compared to that of the PFO

365 model (Table 1). Hence, the adsorption process of Cu(II) and Cr(VI) onto HS-PVC could be

366 well described by the PSO model, indicating that chemisorption might be the rate-limiting

367 step. In addition, more active sites were reported with the PSO model compared to the PFO

368 model (Wang and Guo 2020), which was crucial to the adsorption of Cu(II) and Cr(VI) onto

369 HS-PVC.

370 Adsorption isotherms play a crucial role in investigating the chemical interactions

371 between adsorbates and adsorbents (Yang et al., 2019, Wang and Guo 2020). The adsorption

372 isotherms of the adsorption of Cu(II) and Cr(VI) onto HS-PVC at three different temperatures

373 (25, 35, and 45°C) were shown in Fig. 5C-5F. During the adsorption of Cu(II), the R^2 values

374 of the Langmuir model (0.94–0.96) were higher than those of the Freundlich model (0.82–

375 0.89) at all tested temperatures (25, 35, and 45 °C) (Fig. 5C, 5D, and Table S4), indicating

376 that the adsorption of Cu(II) by HS-PVC was a monolayer process. Similarly, the adsorption

377 of Cr(VI) was also a monolayer process due to the higher R^2 values of the Langmuir model

378 (0.94 at 25 °C and 0.95 at 35 °C) compared to those of the Freundlich model (0.90 at 25 °C

379 and 0.89 at 35 °C) (Fig. 5E, 5F, and Table S4). However, the adsorption of Cr(VI) was fitted

380 by the Langmuir and Freundlich model equally well according to R^2 values of 0.96 at 45°C.

381 In addition, the values of K_F and q_m increased with the increasing temperature (Table S4),

382 indicating an endothermic adsorption process (Xu et al., 2019).

3.5. Mechanisms for the adsorption of Cu(II) and Cr(VI) onto HS-PVC

384 The removal efficiency of Cu(II) decreased ($p<0.01$) by 19.9 % with the co-adsorption

385 of Cr(VI), and that of Cr(VI) also significantly decreased ($p<0.01$) by 48.8% with the

386 co-adsorption of Cu(II) (Fig. 6A). The selectivity of Cu(II) ($\alpha_{Cr(VI)}^{Cu(II)}= 4.11$) was higher than that

387 of Cr(VI) ($\alpha_{Cr(VI)}^{Cu(II)}= 0.24$) in binary-component solution, indicating that Cu(II) can occupy

388 adsorption sites more easily than Cr(VI). However, during the preloading test, the removal

389 efficiency of Cu(II) decreased by 70.5% using Cr(VI) loaded HS-PVC, which was similar to

390 the decrease in Cr(VI) removal (65.8%) using Cu(II) loaded HS-PVC (Fig. 6A). These results

391 suggested that the Cu(II) and Cr(VI) adsorption might share similar adsorption sites on

392 HS-PVC. The zeta potential, an important index for the electric potential at the mineral

393 surface (Ramasamy et al., 2017, Gu et al., 2021), significantly decreased after HT and

394 sulfonation (Fig. S7). The value increased after the adsorption of Cu(II) (Fig. 6B), indicating

395 electrostatic adsorption (Fig. 7). However, only a slight increase in zeta potential was

396 observed after the Cr(VI) adsorption, implying that other mechanisms govern Cr(VI)

397 adsorption onto HS-PVC.

398   To further explore the mechanism of the adsorption of Cr(VI) onto HS-PVC, XPS

399   analysis was used to investigate the adsorption behavior of hydrochar. The C1s XPS spectra

400   were separated, and the characteristic C=C, C-C, C-O, and C=O bonds were quantified in

401   HS-PVC before and after Cr(VI) adsorption. The intensity of C=C in HS-PVC decreased

402   from 35.5% (Fig. 6C) to 28.5% (Fig. 6D) after adsorption of Cr(VI) (Fig. 6C), suggesting the

403   involvement of this bond in Cr(VI) removal. According to solid-state ^{13}C NMR, aromatic

404   functional groups decreased from 55.0% (Fig. 6 E) to 51.4% (Fig. 6F) after Cr(VI) adsorption,

405   also supporting a decrease of C=C intensity after the adsorption of Cr(VI). In addition, the

406   degree of graphitization of HS-PVC decreased after Cr(VI) adsorption according to the

407   decrease in the ratio of I_G/I_D from 0.77 to 0.73 (Fig. 6G), which might be related to the

408   reduction of Cr(VI). Interestingly, Cr(III) was detected in HS-PVC after the adsorption of

409   Cr(VI) (Fig. 6H). These results indicated that the functional group C=C and aromatic groups

410   might reduce Cr(VI) to Cr(III). In addition, there were shifts of the ring vibration peak in the

411   FTIR spectra after adsorption of Cr(VI) (arrows in Fig. 6I). Since a ligand aligns itself to a

412   metal, the energy of the ligand material will most likely be perturbed, leading ultimately to

413   subtle shifts in the absorption peaks (Sergios et al., 2010). Thus, HS-PVC might also bind

414   Cr(VI), which was consistent with Cr(III) and Cr(VI) in Fig. 6H. It has been reported that

415   Cr(VI) was complexed with phenolic -OH using hydrochar derived from leaves and wood

416   sticks. The adsorbed Cr(VI) was subsequently reduced to Cr(III) by the hydrochar along with

417   the decrease of the functional group C=C (Chen et al., 2017, Chen et al., 2021). In this study,

418   the Cr(VI) was supposed to be complexed by the phenolic -OH (Fig. 6I) existed in HS-PVC

419 and reduced by the C=C in the aromatic structure formed by HT (Fig. 7).

420 Note that the removal efficiency of Cr(VI) significantly decreased from $63.8 \pm 2.0\%$ in

421 the presence of K(I) to $28.2 \pm 5.1\%$ after K(I) was precipitated by $HClO_4$ (Fig. S8). The

422 introduction of H^+ ions increased the proportion of H_2CrO_4, thereby breaking the equilibrium

423 balance of $HCrO_4^-$ and $Cr_2O_7^{2-}$ due to negative charges. This, in turn, suggested that K(I) ions

424 might neutralize the negatively charged HS-PVC surface, thereby facilitating the binding of

425 dichromate ions on HS-PVC (Fig. 7).

426 **3.6. Versatility of HS-PVC**

427 Natural water contains ions and organic compounds (Jeon et al., 2020), which might

428 hinder Cu(II) and Cr(VI) removal by HS-PVC. Due to the competitive adsorption of

429 co-existing ions, the efficient removal of Cu(II) and Cr(VI) decreased only by 19.2% and 25.0%

430 (Fig. 8), respectively, indicating low interference. In addition, HS-PVC was particularly

431 suitable for the removal efficiencies of Cu(II) and Cr(VI) at low concentrations (20 mg/L)

432 ($99.6 \pm 0.1\%$ and $94.3 \pm 2.5\%$, respectively) (Fig. 8). Further, the removal efficiencies of Cu(II)

433 and Cr(VI) using HS-PVC from waste pipes increased by 13.7% and 43.9% (Fig. 8), which

434 were higher than those of HS-PVC derived from PVC powder (Fig. 1). The better performance

435 of HS-PVC (pipes) might be attributed to plasticizers and mineral fillers in the PVC (Correa et

436 al., 2019). The removal efficiencies of other metals such as Mn(II), Cd(II), Ni(II), and Co(II)

437 amounted to $81.2 \pm 2.3\%$, $80.8 \pm 1.7\%$, $70.8 \pm 1.8\%$, and $70.1 \pm 3.2\%$ (Fig. S9), respectively,

438 indicating that HS-PVC is suitable for the treatment of complex industrial wastewater.

439 Moreover, the adsorption of Cu(II) and Cr(VI) decreased only by 10.0% and 31.0% (Fig. S10)

440 after three adsorption-desorption cycles (1 mol/L HCl as eluent), indicating excellent

441 recyclability.

442   Previous studies commonly focused on the conversion of waste PVC into

443 coal-alternative fuel (Lu et al., 2020) or lighter oil (Maity et al., 2020). Using HT and

444 sulfonation modifications, the present study provided a novel strategy for resource recovery

445 of PVC waste by producing efficient adsorbents for Cu(II) cations and Cr(VI) anions removal.

446 The sulfonation intensity was mild in this study (98% sulfuric acid at 70°C). Fuming H_2SO_4,

447 $ClSO_3H$, aryldiazonium sulfonates, and higher temperatures (80–150°C) could be considered

448 for additional optimization. In addition, as it is a "sulfonated carbon" (Konwar et al., 2019),

449 HS-PVC may show promising catalytic performances in various organic transformations,

450 including esterifications, ester exchange (transesterifications), acetalization, etherifications,

451 condensation, and multi-component organic reactions that should be studied in the future.

452 **4. Conclusion**

453   This study provided a novel method to fabricate efficient adsorbent (HS-PVC) from

454 waste PVC for both Cu(II) cations and Cr(VI) anions removal. The removal efficiencies of

455 Cu(II) and Cr(VI) using HS-PVC reached $81.2 \pm 1.6\%$ and $60.3 \pm 3.8\%$, respectively. The first

456 stage of HT was crucial for the dichlorination of PVC and the formation of an aromatic

457 structure, guaranteeing the introduction of $-SO_3H$ onto PVC-derived hydrochar through

458 subsequent sulfonation. In addition, sulfonation also significantly increased the hydrophilicity

459 of HS-PVC. The adsorption of Cu(II) was sensitive to HT temperature, while that of Cr(VI)

460 was more sensitive to HT time. Adsorption isotherm data were accurately fitted by the

461 Langmuir isotherm model with a maximum adsorption capacity of 48.9 mg/g for the

462 adsorption of Cu(II) and 20.2 mg/g for the adsorption of Cr(VI) at 45°C. Competitive

463 adsorption of Cu(II) and Cr(VI) occurred, and the selectivity of HS-PVC for the removal of

464 Cu(II) was higher than that of Cr(VI). The adsorption mechanism of Cu(II) was electrostatic

465 adsorption, while Cr(VI) were possibly complexed by the phenolic -OH and reduced to Cr(III)

466 cations by C=C groups in HS-PVC. In addition, HS-PVC was particularly suitable for the

467 adsorption of both metals at low concentrations (＞94% at 20 mg/L). HS-PVC derived from

468 PVC waste pipes also showed high absorption efficiencies for Cu(II) and Cr(VI) (＞90%).

469

475

476 **References**

477 Adam, M.C., Oscar, M.R.-N., Ayomi, J., Gehan De, S., Mahinda, I.R., Ashantha, G.,
478 Erick, R.B., 2020, Influence of surface hydrophobicity/hydrophilicity of biochar on the
479 removal of emerging contaminants. Chem. Eng. J.
480 http://dx.doi.org/10.1016/j.cej.2020.126277.
481 Ahsan, M.A., Katla, S.K., Islam, M.T., Hernandez-Viezcas, J.A., Martinez, L.M.,
482 Diaz-Moreno, C.A., Lopez, J., Singamaneni, S.R., Banuelos, J., Gardea-Torresdey, J., Noveron,
483 J.C., 2018, Adsorptive removal of methylene blue, tetracycline and Cr(VI) from water using
484 sulfonated tea waste. Environmental Technology & Innovation 11, 23-40.
485 http://dx.doi.org/10.1016/j.eti.2018.04.003.
486 Azzaz, A.A., Khiari, B., Jellali, S., Ghimbeu, C.E.M., Jeguirim, M., 2020, Hydrochars
487 production, characterization and application for wastewater treatment: A review. Renew. Sust.

Energ. Rev 127, 109882. http://dx.doi.org/10.1016/j.rser.2020.109882.

Chen, G., Wang, X., Jiang, Y., Mu, X., Liu, H., 2019, Insights into deactivation mechanism of sulfonated carbonaceous solid acids probed by cellulose hydrolysis. Catalysis Today 319, 25-30. http://dx.doi.org/10.1016/j.cattod.2018.03.069.

Chen, N., Cao, S., Zhang, L., Peng, X., Wang, X., Ai, Z., Zhang, L., 2021, Structural dependent Cr(VI) adsorption and reduction of biochar: hydrochar versus pyrochar. Sci. Total. Environ. 783. http://dx.doi.org/10.1016/j.scitotenv.2021.147084.

Chen, N., Huang, Y., Hou, X., Ai, Z., Zhang, L., 2017, Photochemistry of Hydrochar: Reactive Oxygen Species Generation and Sulfadimidine Degradation. Environ. Sci. Technol. 51(19), 11278-11287. http://dx.doi.org/10.1021/acs.est.7b02740.

Correa, C.A., de Santi, C.R., Leclerc, A., 2019, Green-PVC with full recycled industrial waste and renewably sourced content. Journal of Cleaner Production 229, 1397-1411. http://dx.doi.org/10.1016/j.jclepro.2019.04.383.

Cui, X., Zhang, J., Pan, M., Lin, Q., Khan, M.B., Yang, X., He, Z., Yan, B., Chen, G., 2021, Double-edged effects of polyvinyl chloride addition on heavy metal separation and biochar production during pyrolysis of Cd/Zn hyperaccumulator. Journal of Hazardous Materials. http://dx.doi.org/10.1016/j.jhazmat.2021.125793.

Deng, J., Li, X., Wei, X., Liu, Y., Liang, J., Song, B., Shao, Y., Huang, W., 2020, Hybrid silicate-hydrochar composite for highly efficient removal of heavy metal and antibiotics: coadsorption and mechanism. Chem. Eng. J. http://dx.doi.org/10.1016/j.cej.2020.124097.

Dong, C., Zhang, F., Pang, Z., Yang, G., 2016, Efficient and selective adsorption of multi-metal ions using sulfonated cellulose as adsorbent. Carbohyd. Polym. 151, 230-236. http://dx.doi.org/10.1016/j.carbpol.2016.05.066.

Erdem, C.U., Ateia, M., Liu, C., Karan, T., 2020, Activated carbon and organic matter characteristics impact the adsorption of DBP precursors when chlorine is added prior to GAC contactors. Water Res. 184, 116146. http://dx.doi.org/10.1016/j.watres.2020.116146.

Gu, S., Boase, E.M., Lan, C.Q., 2021, Enhanced Pb(II) removal by green alga Neochloris oleoabundans cultivated in high dissolved inorganic carbon cultures. Chem. Eng. J. 416. http://dx.doi.org/10.1016/j.cej.2021.128983.

Huang, N., Zhao, P., Ghosh, S., Fedyukhin, A., 2019, Co-hydrothermal carbonization of polyvinyl chloride and moist biomass to remove chlorine and inorganics for clean fuel production. Appl. Energ. 240, 882-892. http://dx.doi.org/10.1016/j.apenergy.2019.02.050.

Jeon, C., Solis, K.L., An, H.-R., Hong, Y., Igalavithana, A.D., Ok, Y.S., 2020, Sustainable removal of Hg(II) by sulfur-modified pine-needle biochar. Journal of Hazardous Materials 388. http://dx.doi.org/10.1016/j.jhazmat.2020.122048.

Jiang, G., Monsalve, D.A.S., Clough, P., Jiang, Y., Leeke, G.A., 2021, Understanding the Dechlorination of Chlorinated Hydrocarbons in the Pyrolysis of Mixed Plastics. Acs Sustain. Chem. Eng. 9(4), 1576-1589. http://dx.doi.org/10.1021/acssuschemeng.0c06461.

Kawecki, D., Nowack, B., 2019, Polymer-Specific Modeling of the Environmental Emissions of Seven Commodity Plastics As Macro- and Microplastics. Environ. Sci. Technol. 53(16), 9664-9676. http://dx.doi.org/10.1021/acs.est.9b02900.

Kazak, O., Tor, A., 2020, In situ preparation of magnetic hydrochar by co-hydrothermal

treatment of waste vinasse with red mud and its adsorption property for Pb(II) in aqueous solution. Journal of Hazardous Materials 393. http://dx.doi.org/10.1016/j.jhazmat.2020.122391.

Konwar, L.J., Maki-Arvela, P., Mikkola, J.-P., 2019, SO3H-Containing Functional Carbon Materials: Synthesis, Structure, and Acid Catalysis. Chem. Rev. 119(22), 11576-11630. http://dx.doi.org/10.1021/acs.chemrev.9b00199.

Kunwar, B., Cheng, H.N., Chandrashekaran, S.R., Sharma, B.K., 2016, Plastics to fuel: a review. Renew. Sust. Energ. Rev 54, 421-428. http://dx.doi.org/10.1016/j.rser.2015.10.015.

Lau, W.W.Y., Shiran, Y., Bailey, R.M., Cook, E., Stuchtey, M.R., Koskella, J., Velis, C.A., Godfrey, L., Boucher, J., Murphy, M.B., Thompson, R.C., Jankowska, E., Castillo, A.C., Pilditch, T.D., Dixon, B., Koerselman, L., Kosior, E., Favoino, E., Gutberlet, J., Baulch, S., Atreya, M.E., Fischer, D., He, K.K., Petit, M.M., Sumaila, U.R., Neil, E., Bernhofen, M.V., Lawrence, K., Palardy, J.E., 2020, Evaluating scenarios toward zero plastic pollution. Science 369(6510), 1455-1461. http://dx.doi.org/10.1126/science.aba9475.

Li, F., Zimmerman, A.R., Hu, X., Gao, B., 2020, Removal of aqueous Cr(VI) by Zn- and Al-modified hydrochar. Chemosphere 260, 127610-127610. http://dx.doi.org/10.1016/j.chemosphere.2020.127610.

Li, X., Wang, J., You, J., Yu, P., Li, X., Xue, G., Chen, H., Xu, X., van Agtmaal, S., Alvarez, P.J.J., 2019, Hazardous waste dewatering and dry mass reduction through hydrophobic modification by a facile one-pot, alkali-assisted hydrothermal reaction. Water Res. 155, 225-232. http://dx.doi.org/10.1016/j.watres.2019.02.050.

Liu, Y., Zhou, C., Li, F., Liu, H., Yang, J., 2020, Stocks and flows of polyvinyl chloride (PVC) in China: 1980-2050. Resour. Conserv. Recy. 154, 104584. http://dx.doi.org/10.1016/j.resconrec.2019.104584.

Lu, X., Ma, X., Chen, X., Yao, Z., Zhang, C., 2020, Co-hydrothermal carbonization of polyvinyl chloride and corncob for clean solid fuel production. Bioresource. Technol. 301, 122763. http://dx.doi.org/10.1016/j.biortech.2020.122763.

Ma, D., Feng, Q., Chen, B., Cheng, X., Chen, K., Li, J., 2019, Insight into chlorine evolution during hydrothermal carbonization of medical waste model. Journal of Hazardous Materials. http://dx.doi.org/10.1016/j.jhazmat.2019.120847.

Maity, A., Chaudhari, S., Titman, J.J., Polshettiwar, V., 2020, Catalytic nanosponges of acidic aluminosilicates for plastic degradation and CO2 to fuel conversion. Nature Commun. 11(1), 1-12. http://dx.doi.org/10.1038/s41467-020-17711-6.

Matthews, C., Moran, F., Jaiswal, A.K., 2021, A review on European Union's strategy for plastics in a circular economy and its impact on food safety. Journal of Cleaner Production 283. http://dx.doi.org/10.1016/j.jclepro.2020.125263.

Miao, F., Liu, Y., Gao, M., Yu, X., Xiao, P., Wang, M., Wang, S., Wang, X., 2020, Degradation of polyvinyl chloride microplastics via an electro-Fenton-like system with a TiO2/graphite cathode. Journal of Hazardous Materials. http://dx.doi.org/10.1016/j.jhazmat.2020.123023.

Ning, X., Teng, H., Wang, G., Zhang, J., Zhang, N., Huang, C., Wang, C., 2020, Physiochemical, structural and combustion properties of hydrochar obtained by hydrothermal

carbonization of waste polyvinyl chloride. Fuel 270, 117526. http://dx.doi.org/10.1016/j.fuel.2020.117526.

Park, J.-H., Ok, Y.S., Kim, S.-H., Cho, J.-S., Heo, J.-S., Delaune, R.D., Seo, D.-C., 2016, Competitive adsorption of heavy metals onto sesame straw biochar in aqueous solutions. Chemosphere 142, 77-83. http://dx.doi.org/10.1016/j.chemosphere.2015.05.093.

Poerschmann, J., Weiner, B., Woszidlo, S., Koehler, R., Kopinke, F.D., 2015, Hydrothermal carbonization of poly(vinyl chloride). Chemosphere 119, 682-689. http://dx.doi.org/10.1016/j.chemosphere.2014.07.058.

Ramasamy, D.L., Repo, E., Srivastava, V., Sillanpaa, M., 2017, Chemically immobilized and physically adsorbed PAN/acetylacetone modified mesoporous silica for the recovery of rare earth elements from the waste water-comparative and optimization study. Water Res. 114, 264-276. http://dx.doi.org/10.1016/j.watres.2017.02.045.

Rueda-Marquez, J.J., Moreno-Andres, J., Rey, A., Corada-Fernandez, C., Mikola, A., Manzano, M.A., Levchuk, I., 2021, Post-treatment of real municipal wastewater effluents by means of granular activated carbon (GAC) based catalytic processes: A focus on abatement of pharmaceutically active compounds. Water Res. 192, 116833-116833. http://dx.doi.org/10.1016/j.watres.2021.116833.

Sergios, K.P., Evangelos, P.K., Evangelos, P.F., Andreas, A.S., George, E.R., Fotios, K.K., 2010, Metal-carboxylate interactions in metal-alginate complexes studied with FTIR spectroscopy. Carbohyd. Res. http://dx.doi.org/10.1016/j.carres.2009.12.010.

Shen, Y., Yu, S., Ge, S., Chen, X., Ge, X., Chen, M., 2017, Hydrothermal carbonization of medical wastes and lignocellulosic biomass for solid fuel production from lab-scale to pilot-scale. Energy 118, 312-323. http://dx.doi.org/10.1016/j.energy.2016.12.047.

Sheng, K., Zhang, S., Liu, J., E, S., Jin, C., Xu, Z., Zhang, X., 2019, Hydrothermal carbonization of cellulose and xylan into hydrochars and application on glucose isomerization. Journal of Cleaner Production 237, 117831. http://dx.doi.org/10.1016/j.jclepro.2019.117831.

Song, J., Zhang, S., Li, G., Du, Q., Yang, F., 2020, Preparation of montmorillonite modified biochar with various temperatures and their mechanism for Zn ion removal. Journal of Hazardous Materials 391. http://dx.doi.org/10.1016/j.jhazmat.2019.121692.

Tong, S., Shen, J., Jiang, X., Li, J., Sun, X., Xu, Z., Chen, D., 2021, Recycle of Fenton sludge through one-step synthesis of aminated magnetic hydrochar for Pb2+ removal from wastewater. Journal of Hazardous Materials 406. http://dx.doi.org/10.1016/j.jhazmat.2020.124581.

Wang, C., Klamerth, N., Messele, S.A., Singh, A., Belosevic, M., El -Din, M.G., 2016, Comparison of UV/hydrogen peroxide, potassium ferrate(VI), and ozone in oxidizing the organic fraction of oil sands process-affected water (OSPW). Water Res. 100, 476-485. http://dx.doi.org/10.1016/j.watres.2016.05.037.

Wang, J., Guo, X., 2020, Adsorption isotherm models: Classification, physical meaning, application and solving method. Chemosphere 258. http://dx.doi.org/10.1016/j.chemosphere.2020.127279.

Wang, J., Guo, X., 2020, Adsorption kinetic models: Physical meanings, applications, and solving methods. Journal of Hazardous Materials 390.

614 http://dx.doi.org/10.1016/j.jhazmat.2020.122156.

615 Wang, X., Zhan, C., Ding, Y., Ding, B., Xu, Y., Liu, S., Dong, H., 2017, Dual-Core
616 Fe2O3@Carbon Structure Derived from Hydrothermal Carbonization of Chitosan as a Highly
617 Efficient Material for Selective Adsorption. Acs Sustain. Chem. Eng. 5(2), 1457-1467.
618 http://dx.doi.org/10.1021/acssuschemeng.6b02034.

619 Wiedinmyer, C., Yokelson, R.J., Gullett, B.K., 2014, Global Emissions of Trace Gases,
620 Particulate Matter, and Hazardous Air Pollutants from Open Burning of Domestic Waste.
621 Environ. Sci. Technol. 48(16), 9523-9530. http://dx.doi.org/10.1021/es502250z.

622 Xiao, Y., Hill, J.M., 2020, Solid acid catalysts produced by sulfonation of petroleum coke:
623 Dominant   role   of   aromatic   hydrogen.   Chemosphere   248.
624 http://dx.doi.org/10.1016/j.chemosphere.2020.125981.

625 Xiao, Y., Hill, J.M., 2020, Solid acid catalysts produced by sulfonation of petroleum coke:
626 Dominant   role   of   aromatic   hydrogen.   Chemosphere   248,   125981.
627 http://dx.doi.org/10.1016/j.chemosphere.2020.125981.

628 Xu, Y., Chen, J., Chen, R., Yu, P., Guo, S., Wang, X., 2019, Adsorption and reduction of
629 chromium(VI) from aqueous solution using polypyrrole/calcium rectorite composite adsorbent.
630 Water Res. 160, 148-157. http://dx.doi.org/10.1016/j.watres.2019.05.055.

631 Yang, F., Du, Q., Sui, L., Cheng, K., 2021, One-step fabrication of artificial humic
632 acid-functionalized colloid-like magnetic biochar for rapid heavy metal removal. Bioresource.
633 Technol. 328. http://dx.doi.org/10.1016/j.biortech.2021.124825.

634 Yang, F., Zhang, S., Sun, Y., Du, Q., Song, J., Tsang, D.C.W., 2019, A novel
635 electrochemical modification combined with one-step pyrolysis for preparation of sustainable
636 thorn-like   iron-based   biochar   composites.   Bioresource.   Technol.   274,   379-385.
637 http://dx.doi.org/10.1016/j.biortech.2018.10.042.

638 Ye, L., Qi, C., Hong, J., Ma, X., 2017, Life cycle assessment of polyvinyl chloride
639 production and its recyclability in China. Journal of Cleaner Production 142, 2965-2972.
640 http://dx.doi.org/10.1016/j.jclepro.2016.10.171.

641 Yu, J., Sun, L., Ma, C., Qiao, Y., Yao, H., 2016, Thermal degradation of PVC: A review.
642 Waste Manage. 48, 300-314. http://dx.doi.org/10.1016/j.wasman.2015.11.041.

643 Zhang, C.Y., Ma, X.Q., Huang, T., Zhou, Y., Tian, Y.L., 2020, Co-hydrothermal
644 carbonization of water hyacinth and polyvinyl chloride: Optimization of process parameters
645 and   characterization   of   hydrochar.   Bioresource.   Technol.   314,   123676.
646 http://dx.doi.org/10.1016/j.biortech.2020.123676.

647
648

649 **Table 1**

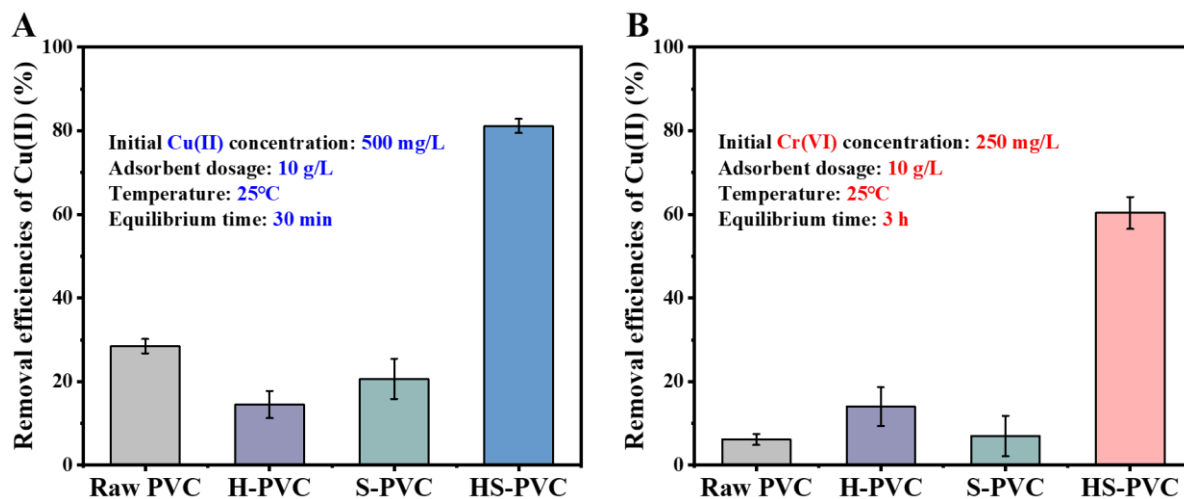650 PFO and PSO model parameters for Cu(II) and Cr(VI) adsorption onto HS-PVC.

Metals	q_{exp} (mg/g)	PFO			PSO		
		q_1 (mg/g)	R_1^2	k_1 (min^{-1})	q_2 (mg/g)	R_2^2	k_2 (g/(mg·min))
Cu(II)	40.34	38.18	0.86	17.92	40.24	0.95	0.70
Cr(VI)	17.75	15.41	0.88	2.39	16.23	0.94	0.25

651

652

653

654

A

Removal efficiencies of Cu(II) (%)

Initial **Cu(II)** concentration: **500 mg/L**
Adsorbent dosage: **10 g/L**
Temperature: **25°C**
Equilibrium time: **30 min**

Raw PVC H-PVC S-PVC HS-PVC

B

Removal efficiencies of Cu(II) (%)

Initial **Cr(VI)** concentration: **250 mg/L**
Adsorbent dosage: **10 g/L**
Temperature: **25°C**
Equilibrium time: **3 h**

Raw PVC H-PVC S-PVC HS-PVC

655

656 Fig. 1. Cu(II) and Cr(VI) removal efficiencies using Raw PVC, H-PVC, S-PVC, and

657 HS-PVC after adsorption for 12 hours.

658
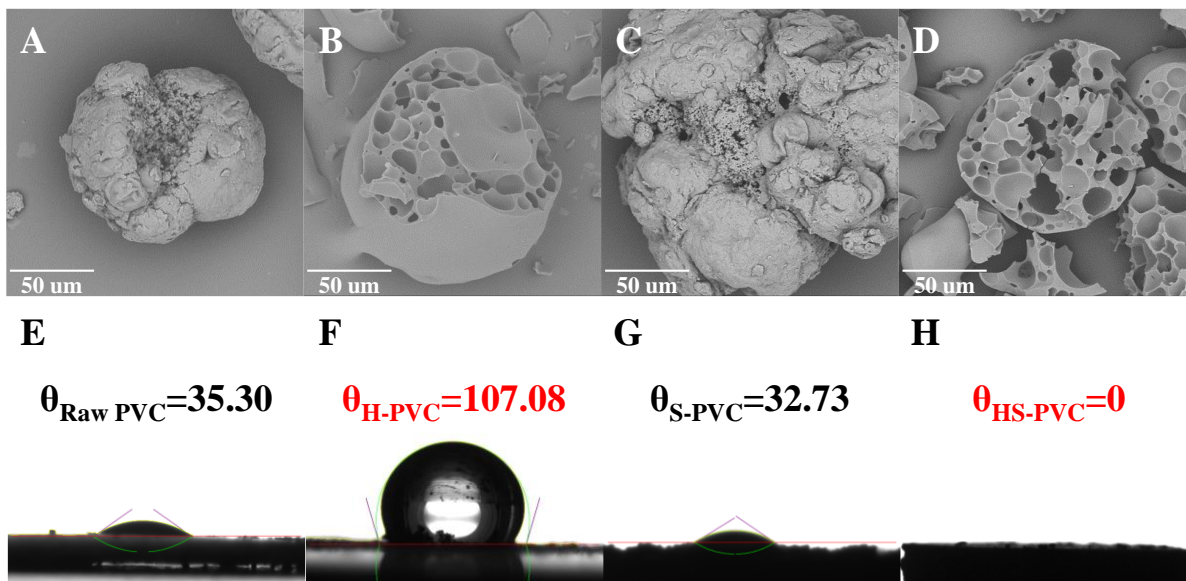
659

660 Fig. 2. Surface properties of PVC derived adsorbents: SEM images of Raw PVC (A), H-PVC

661 (B), S-PVC (C), and HS-PVC (D); contact angle (θ) of Raw PVC (E), H-PVC (F), S-PVC

662 (G), and HS-PVC (I).

663

664
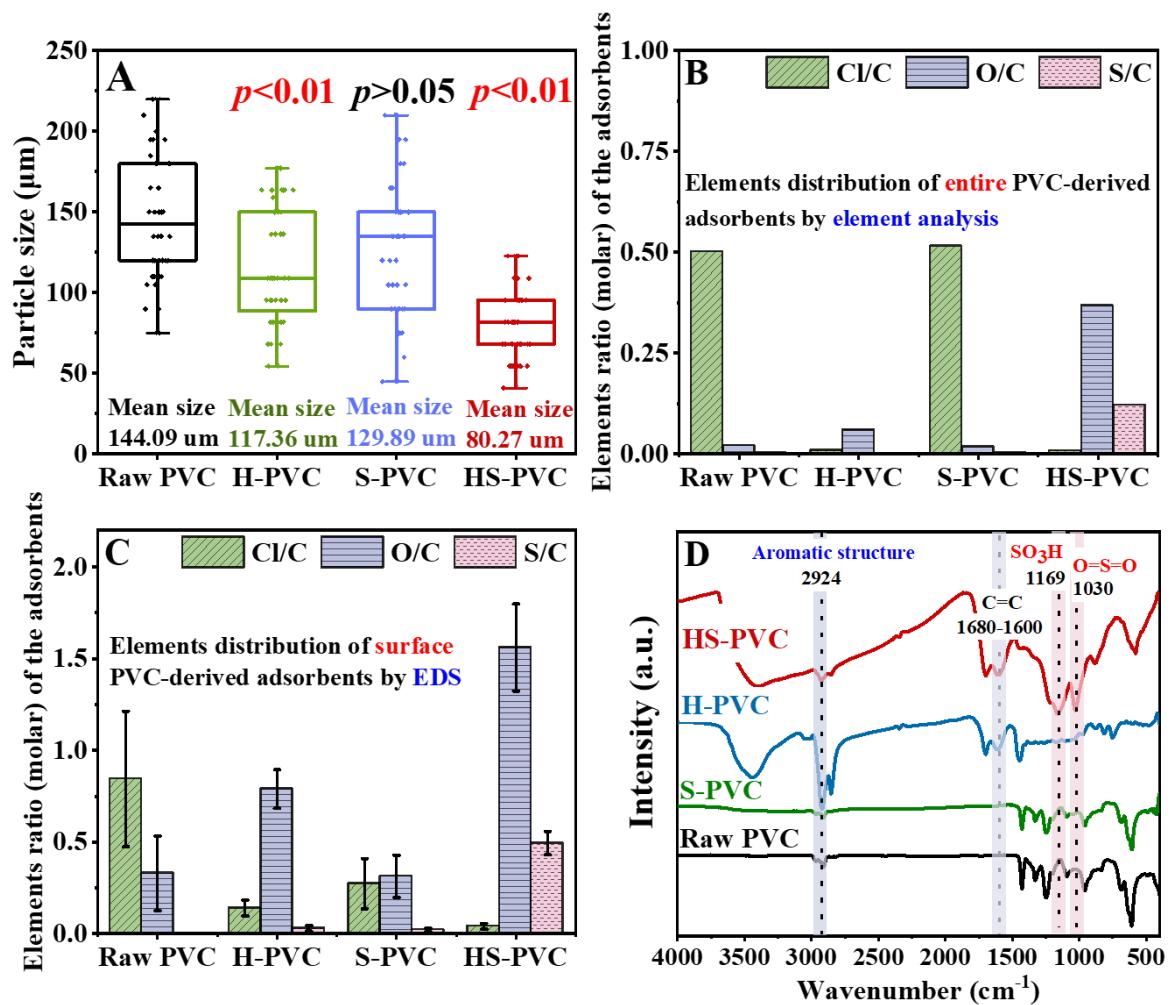
Fig. 3. Characterization of Raw PVC, H-PVC, S-PVC, and HS-PVC: particle size distribution

(A), elemental analysis (B), EDS element mapping (C), and FTIR spectra (D).
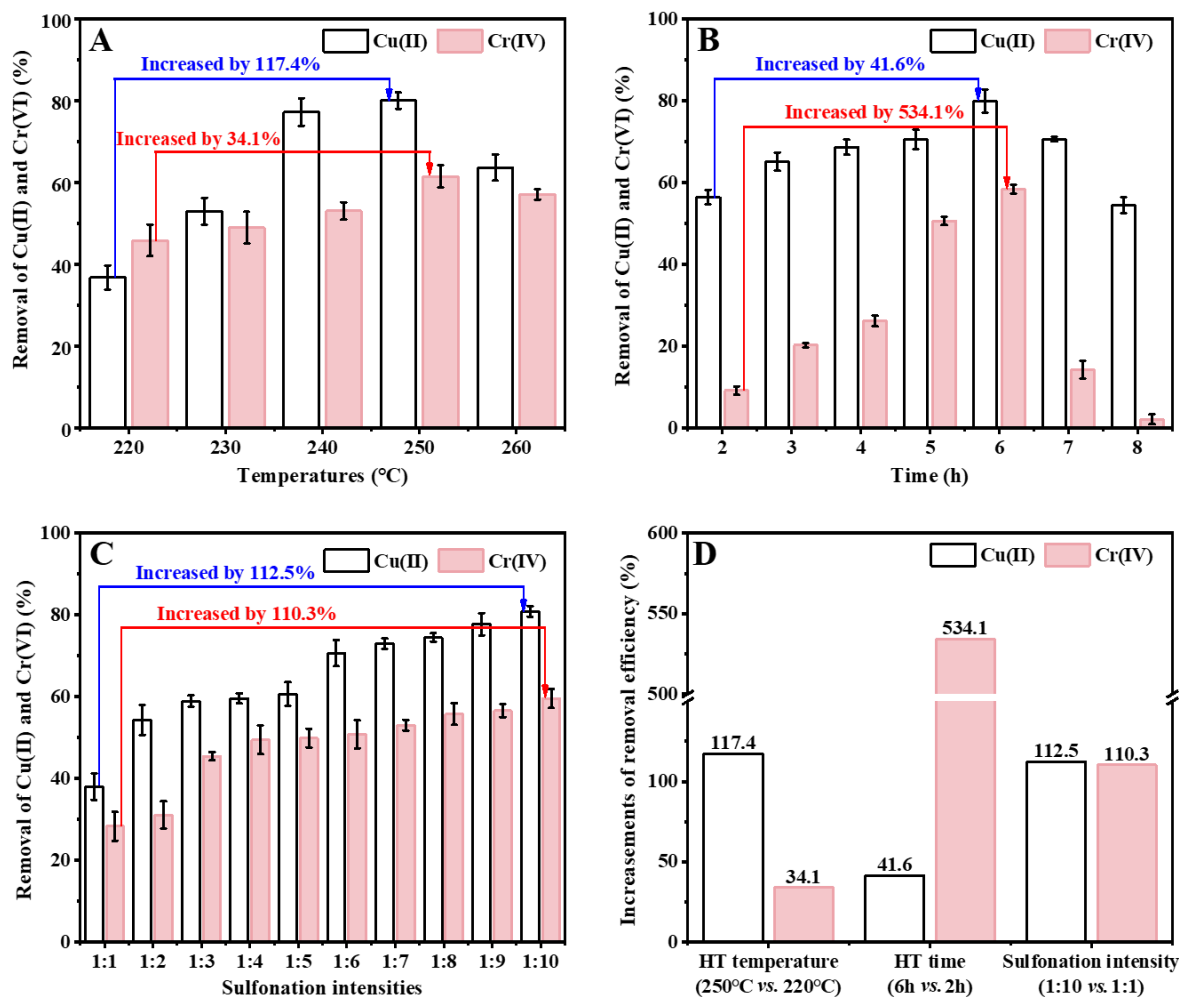
Fig. 4. Effects of HS-PVC preparation intensities on Cu(II) and Cr(VI) removal: HT temperature (A), HT time (B), sulfonation intensity (C), and comparison of Cu(II) and Cr(VI) removal efficiencies between the optimal and the lowest efficiency (D) (HT temperature: 250 °C *vs.* 220 °C, HT time: 6 h *vs.* 2 h, and sulfonation intensity: 1:10 *vs.* 1:1). The initial concentrations of Cu(II) and Cr(VI) were 500 and 250 mg/L. The adsorbent dose was 10 g/L and the temperature 25 °C.
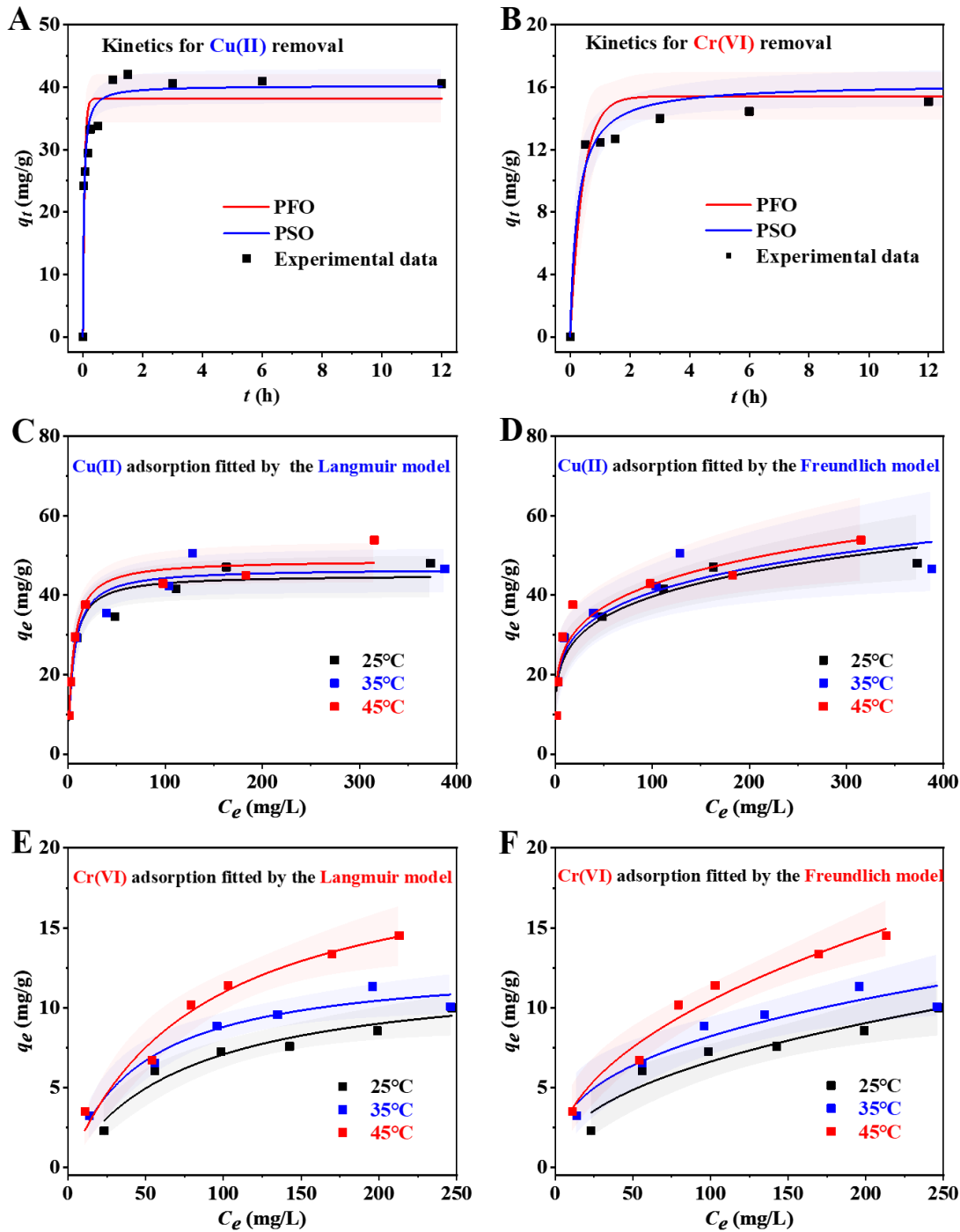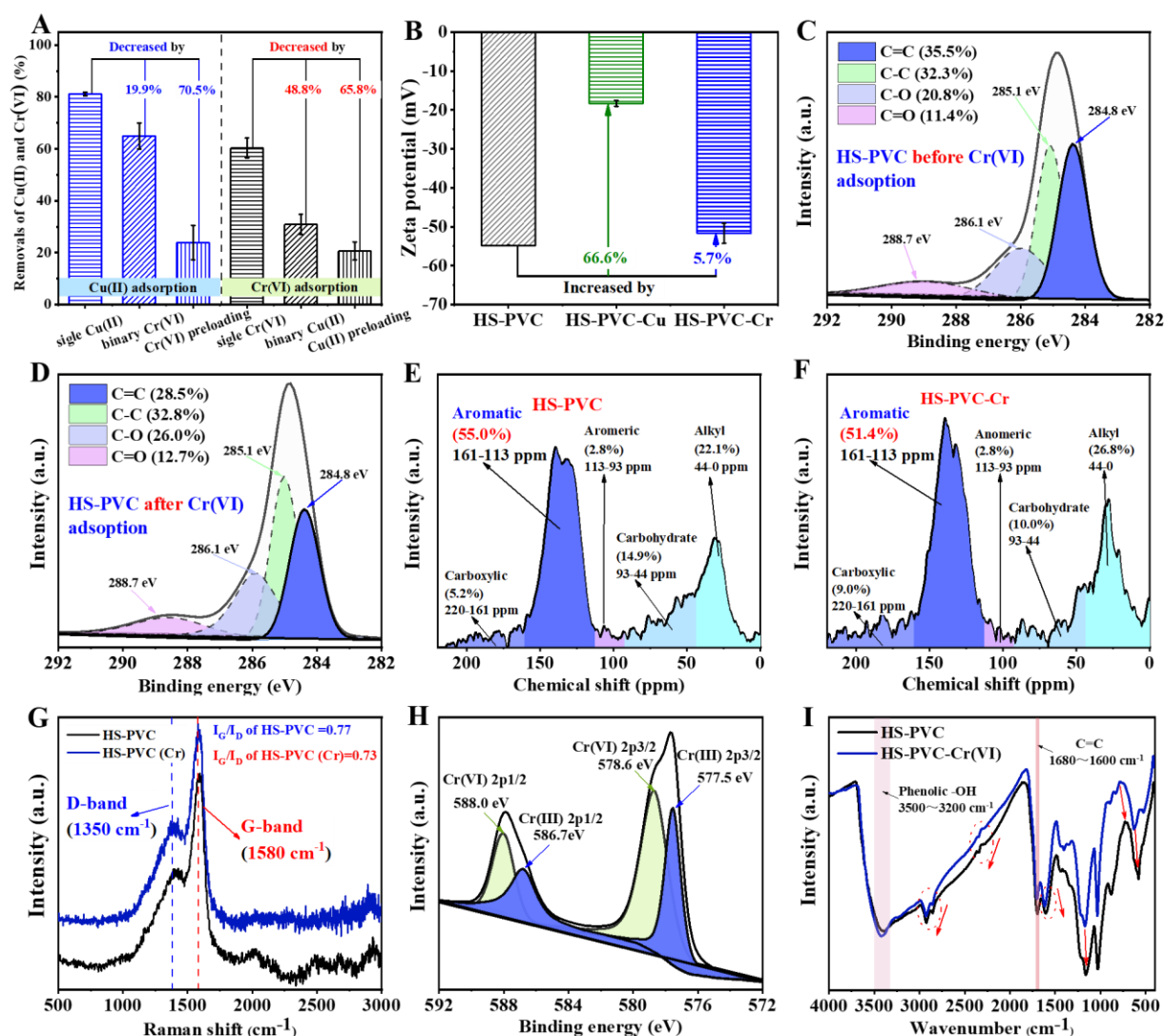
Fig. 5. Adsorption kinetics of Cu(II) (A) and Cr(VI) (B) onto HS-PVC. Equilibrium isotherms of Cu(II) fitted by the Langmuir (C) and Freundlich models (D) at different temperatures (25, 35, and 45 °C). Equilibrium isotherms of Cr(VI) fitted by the Langmuir (E) and Freundlich models (F) at different temperatures (25, 35, and 45 °C). The colored area covers the 95% confidence intervals.

Fig. 6. Mechanisms for the adsorptions of Cu(II) and Cr(VI) by HS-PVC. Competitive adsorption between Cu(II) and Cr(VI) by HS-PVC (A). Zeta potential of HS-PVC, HS-PVC after the adsorption of Cu(II) (HS-PVC-Cu), and HS-PVC after the adsorption of Cr(VI) (HS-PVC-Cr) (B). C 1s XPS spectra of HS-PVC before the adsorption of Cr(VI) (C) and after the adsorption of Cr(VI) (D). Solid-state ^{13}C NMR of HS-PVC before the adsorption of Cr(VI) (E) and after the adsorption of Cr(VI) (F). Raman spectra of HS-PVC before and after adsorption of Cr(VI) (a higher $I_G/I_D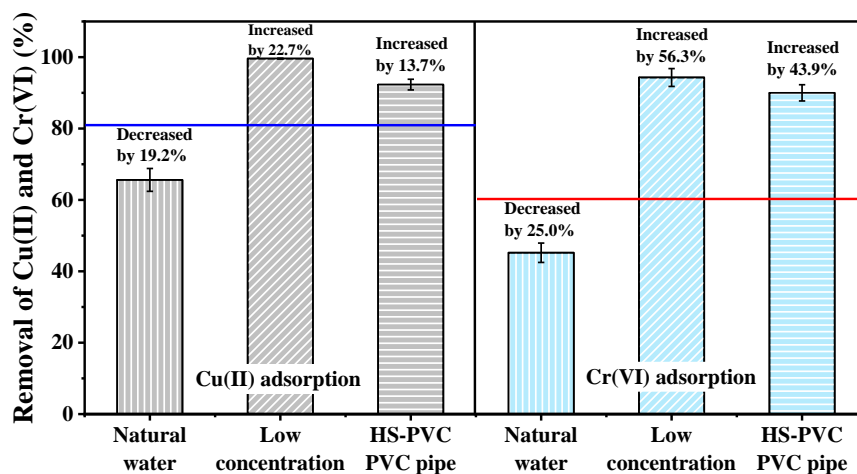$ ratio indicates a higher degree of graphitization) (G). Cr 2p XPS spectra of HS-PVC after the adsorption of Cr(VI) (H). FTIR spectra of HS-PVC before and after the adsorption of Cr(VI) (I).
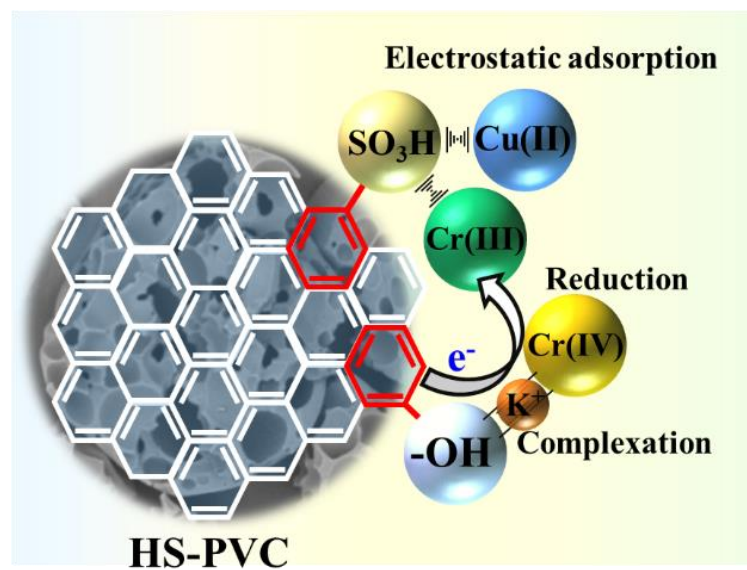
692
693   Fig. 7. Schematic adsorption of Cu(II) and Cr(VI) using HS-PVC
694

695

696   Fig. 8. Versatility of HS-PVC for Cu(II) and Cr(VI) removal efficiencies. Removal of

697   Cu(II) and Cr(VI) by HS-PVC from natural water, at low concentration (20 mg/L), and by

698   HS-PVC derived from waste PVC pipes (blue and red lines represent the removal efficiency

699   of Cu(II) and Cr(VI) by PVC powder in Fig. 1).

700

701